Remineralization dominating the $\delta^{13}C$ decrease in the mid-depth Atlantic during the last deglaciation

Sifan Gu[1,2], Zhengyu Liu[3], Delia W. Oppo[4], Jean Lynch-Stieglitz[5], Alexandra Jahn[6], Jiaxu Zhang[7,8], Keith Lindsay[9], Lixin Wu[10]

[1] School of Oceanography, Shanghai Jiao Tong University, Shanghai, China
[2] Open Studio for Ocean-Climate-Isotope Modeling, Pilot National Laboratory for Marine Science and Technology (Qingdao), Qingdao, China
[3] Atmospheric Science Program, Department of Geography, The Ohio State University, Columbus, OH, USA
[4] Department of Geology and Geophysics, Woods Hole Oceanographic Institution, Woods Hole, MA, USA
[5] School of Earth and Atmospheric Sciences, Georgia Institute of Technology, Atlanta, Georgia, USA
[6] Department for Atmospheric and Oceanic Sciences and Institute of Arctic and Alpine Research, University of Colorado Boulder, Boulder, CO, USA
[7] Cooperative Institute for Climate, Ocean, and Ecosystem Studies, University of Washington, Seattle, WA, USA
[8] NOAA Pacific Marine Environmental Laboratory, Seattle, WA, USA
[9] National Center for Atmospheric Research, Climate and Global Dynamics Division, Boulder, CO, USA
[10] Physical Oceanography Laboratory, Ocean University of China, Qingdao, China

Corresponding authors: Sifan Gu (gusifan@stju.edu.cn), Zhengyu Liu (liu.7022@osu.edu)

Highlights:

- Increased South Sourced Water in the mid-depth Atlantic during HS1 plays a minor role in the $\delta^{13}C$ decrease.
- Remineralization caused by the change of ventilation dominates the deglacial $\delta^{13}C$ change.
- Deep end-member includes additional remineralization after the surface end-member leaves the surface.

Keywords:
$\delta^{13}C$, water mass composition, remineralization, end-member, HS1

An edited and typeset version of this manuscript is published as:

Sifan Gu, Zhengyu Liu, Delia W. Oppo, Jean Lynch-Stieglitz, Alexandra Jahn, Jiaxu Zhang, Keith Lindsay, Lixin Wu (2021), Remineralization dominating the δ13C decrease in the mid-depth Atlantic during the last deglaciation, Earth and Planetary Science Letters, 571, https://doi.org/10.1016/j.epsl.2021.117106.

Abstract

$\delta^{13}C$ records from the mid-depth Atlantic show a pronounced decrease during the Heinrich Stadial 1 (HS1), a deglacial episode of dramatically weakened Atlantic Meridional Ocean Circulation (AMOC). Proposed explanations for this mid-depth decrease include a greater fraction of $\delta^{13}C$-depleted southern sourced water (SSW), a $\delta^{13}C$ decrease in the North Atlantic Deep Water (NADW) end-member, and accumulation of the respired organic carbon. However, the relative importance of these proposed mechanisms cannot be quantitatively constrained from current available observations alone. Here we diagnose the individual contributions to the deglacial Atlantic mid-depth $\delta^{13}C$ change from these mechanisms using a transient simulation with carbon isotopes and idealized tracers. We find that although the fraction of the low-$\delta^{13}C$ SSW increases in response to a weaker AMOC during HS1, the water mass mixture change only plays a minor role in the mid-depth Atlantic $\delta^{13}C$ decrease. Instead, increased remineralization due to the AMOC-induced mid-depth ocean ventilation decrease is the dominant cause. In this study, we differentiate between the deep end-members, which are assigned to deep water regions used in previous paleoceanography studies, and the surface end-members, which are from the near-surface water defined from the physical origin of deep water masses. We find that the deep NADW end-member includes additional remineralized material accumulated when sinking from the surface (surface NADW end-member). Therefore, the surface end-members should be used in diagnosing mechanisms of $\delta^{13}C$ changes. Furthermore, our results suggest that remineralization in the surface end-member is more critical than the remineralization along the transport pathway from the near-surface formation region to the deep ocean, especially during the early deglaciation.

1. Introduction

The climate experienced significant changes during the last deglaciation. One key event is the Heinrich Stadial 1 (HS1) (17.5-14.7 ka BP) when the Atlantic Meridional Overturning Circulation (AMOC) is nearly collapsed (McManus et al., 2004) or significantly weakened (Gherardi et al., 2009). During HS1, the atmospheric CO_2 increased by 35 ppmv and the $\delta^{13}C$ of CO_2 decreased by 0.3‰, which is suggested to be released from the ocean (Bauska et al., 2016; Schmitt et al., 2012). At the same time, the marine $\delta^{13}C$ reconstructions show a widespread $\delta^{13}C$ decrease in the mid-depth (1500-2500m) Atlantic (e.g. Lund et al., 2015; Oppo et al., 2015; Tessin & Lund, 2013), but it is still highly uncertain what caused this mid-depth $\delta^{13}C$ decrease in the Atlantic.

With reduced North Atlantic Deep Water (NADW) formation during HS1 (McManus et al., 2004), an increased contribution of low-$\delta^{13}C$ southern-sourced water (SSW; mainly comprised of Antarctic Bottom Water, AABW) in the Atlantic is widely believed to have caused the mid-depth $\delta^{13}C$ decrease (Boyle and Keigwin, 1987; Keigwin and Lehman, 1994; Rickaby and Elderfield, 2005; Sarnthein et al., 1994; Zahn et al., 1997). However, recent studies suggest that the $\delta^{13}C$ decrease could be related to reduced ventilation resulting from a weakening of AMOC, which leads to an accumulation of remineralized carbon and $\delta^{13}C$ decrease at mid-depth (Lacerra et al., 2017; Schmittner and Lund, 2015; Voigt et al., 2017). A third view argues that changes in the end-member value inof NADW could also have caused the mid-depth $\delta^{13}C$ decrease (Lund et al., 2015; Oppo et al., 2015). From the Last Glacial Maximum (LGM) to HS1, the end-member $\delta^{13}C$ values decreased by 1‰ in NADW but remained overall stable in SSW, indicating that the Atlantic mid-depth $\delta^{13}C$ decrease could also be caused by a decrease of the end-member value in NADW (Lund et al., 2015; Oppo et al., 2015). The lower $\delta^{13}C$ NADW end-member at HS1 could be caused by the increased water formed by brine rejection in the Nordic seas with lower $\delta^{13}C$ due

88 to reduced air sea gas exchange (Waelbroeck et al., 2011) incorporated into NADW (Dokken and
89 Jansen, 1999; Thornalley et al., 2010). In fact, all three proposed mechanisms described here could
90 contribute to the mid-depth $\delta^{13}C$ decrease based on existing $\delta^{13}C$ and $\delta^{18}O$ records from the
91 Atlantic, but the relative importance of these mechanisms cannot be constrained by $\delta^{13}C$ and $\delta^{18}O$
92 data alone (Oppo et al., 2015). Our knowledge of the water mass composition in the Atlantic during
93 the last deglaciation limits the quantitative assessment of the proposed mechanisms in the Atlantic
94 mid-depth $\delta^{13}C$ decrease during the deglaciation.

95 Isotope-enabled Earth System Models provide a unique opportunity to quantitatively
96 evaluate relative contribution of individual mechanisms in explaining the deglacial mid-depth
97 $\delta^{13}C$ decrease. Using University of Victoria climate model of intermediate complexity under
98 preindustrial climate conditions, Schmittner and Lund (2015) is able to simulate $\delta^{13}C$ decrease in
99 subsurface Atlantic in response to a prolonged idealized AMOC shutdown, which is dominated by
100 the remineralization. However, the Atlantic water masses and the associated $\delta^{13}C$ were quite
101 different at the LGM from their preindustrial state (e.g., Curry and Oppo, 2005), quantitative
102 assessment of the mid-depth $\delta^{13}C$ decrease under the corresponding climate conditions is therefore
103 needed.

104 Here, we provide a quantitative estimation of previously proposed mechanisms in mid-
105 depth $\delta^{13}C$ decrease during HS1 by diagnosing a deglacial simulation with carbon isotopes and
106 idealized tracers that represent water ventilation and water mass composition. We find that
107 although the NADW proportion in the mid-depth Atlantic decreases during HS1, the partial
108 replacement of NADW by SSW is not a key factor; instead, the accumulation of the remineralized
109 $\delta^{13}C$ is the dominant contributor to the Atlantic mid-depth $\delta^{13}C$ decrease.
110

2. Methods

2.1 Model and Experiments

The physical ocean model used is Parallel Ocean Program version 2 (POP2) (Danabasoglu et al., 2012) with a nominal 3° horizontal resolution and 60 vertical layers. The POP2 version used in this study is implemented with several important geotracers for paleoceanography study purposes and has been used in many recent studies to understand intermediate and deep water masses (Gu et al., 2020, 2017; Zhang et al., 2017) as well as AMOC variations (Gu et al., 2019). These geotracers include carbon isotopes (Jahn et al., 2015) and $^{231}Pa/^{230}Th$ (Gu and Liu, 2017), which have been validated with modern seawater observations. To quantify the deep ocean ventilation, two age tracers are implemented: ideal age and idealized ventilation age (Zhang, 2016). The ideal age is set to 0 at the ocean surface and increases with 1 yr/yr in the ocean interior. The idealized ventilation age is similar to the ideal age except that it considers the isolating effect of sea ice; it is not reset to 0 at ice-covered ocean surface but instead is set to values proportional to ice fraction. Therefore, the idealized ventilation age is in general older than the ideal age and is more realistic to represent the "true" water age. Several dye tracers are also implemented to identify water mass composition in the model (Gu et al., 2020). The dye tracers are reset to 1 over specific regions at the ocean surface at each time step and are advected and diffused passively in the ocean interior. Three dye tracers are released over the surface Southern Ocean (south of 34°S, Dye-South), the subtropical Atlantic (34°S-40°N, Dye-Subtropical), and the North Atlantic (north of 40°N, Dye-North).

A transient simulation of the last deglaciation (C-iTRACE) using the isotope-enabled POP2 (Gu et al., 2019) is analyzed in this study. C-iTRACE is forced by the monthly surface forcings (heat flux, freshwater flux, and momentum flux) from a fully coupled transient simulation

(TRACE21K), which simulates many key features of the last deglaciation (e.g., Liu et al., 2009). In TRACE21K, the amount of freshwater flux is constrained by sea level records, and the locations of the freshwater flux are tested in different sensitivity experiments to best match AMOC indicated by $^{231}Pa/^{230}Th$ reconstruction (McManus et al., 2004) and Greenland surface air temperature records (He, 2011; Liu et al., 2009). The surface temperature and salinity are restored to TRACE21K values with the restoring time scale of 10-day and 30-day, respectively (described in detail in Gu et al. 2019). The atmospheric CO_2 is prescribed following Joos & Spahni (2008), and the $\delta^{13}C$ in the atmospheric CO_2 is prescribed following Schmitt et al. (2012). The dust deposition during the LGM is prescribed following Mahowald et al. (2006), and the transient dust field is generated by interpolated between LGM and modern according to the global temperature reconstruction (Shakun et al., 2012). Decadal average at 20ka in C-iTRACE is used as LGM, and decadal average at 15ka in C-iTRACE is used as HS1 in this study.

2.2 $\delta^{13}C$ decomposition in the model

Simulated $\delta^{13}C$ can be decomposed into preformed ($\delta^{13}C_{pre}$) and remineralized ($\delta^{13}C_{rem}$) parts (eq.1) following the apparent oxygen utilization (AOU) based the method in Sarmiento & Gruber, (1996), which is described in the Supplementary Materials (SM). We note that this AOU-based estimation might overestimate the $\delta^{13}C_{rem}$ because this method assumes that the O_2 at the ocean surface is in equilibrium with the atmosphere, which is not necessarily the case especially in high latitudes (Khatiwala et al., 2019).

$$\delta^{13}C_{rem} = \delta^{13}C - \delta^{13}C_{pre} \quad (1)$$

Another way to estimate the remineralized $\delta^{13}C$ is by end-member mixing. Oppo & Fairbanks (1987) propose that if the $\delta^{13}C$ values of the northern and southern end-members are

158 known, and $\delta^{13}C$ is assumed to be conservative, $\delta^{13}C$ in the Atlantic can be used to estimate the
159 water mass mixture. However, there is a growing body of evidence that remineralization leads to
160 non-conservative effects in $\delta^{13}C$ and that the air-sea component of $\delta^{13}C$ ($\delta^{13}C_{as}$), which removes
161 the biological effects in $\delta^{13}C$, is a more conservative tracer (Broecker and Maier-Reimer, 1992;
162 Gu et al., 2020; Lynch-Stieglitz and Fairbanks, 1994). Therefore, the departures of $\delta^{13}C$ from
163 conservative mixing can be used to estimate the remineralized $\delta^{13}C$ if the $\delta^{13}C$ end-member
164 values and the water mass composition are known (Howe et al., 2016; Piotrowski et al., 2005).

165 Here we define the $\delta^{13}C$ due to the conservative mixing as $\delta^{13}C_{cons}$, which can be
166 calculated by

167 $$\delta^{13}C_{cons} = \alpha * \delta^{13}C_S + (1-\alpha) * \delta^{13}C_N \quad (2)$$

168 where α is the fraction of SSW indicated by idealized Dye-South tracer, and $\delta^{13}C_S$ and $\delta^{13}C_N$ are
169 the end-member values from south and north, respectively. To estimate the relative contribution
170 of changes in water mass composition and end-member values on $\delta^{13}C_{cons}$, we further split the
171 change in $\delta^{13}C_{cons}$ into different components based on Eq.2, including the change due to water
172 mass fraction ($\delta^{13}C_{cons-frac}$), end-member change ($\delta^{13}C_{cons-end}$), and the non-linear term
173 ($\delta^{13}C_{cons-nonlinear}$) (eq.3):

174 $$\delta'_{cons} = \underbrace{\alpha'\overline{\delta_S} + \left(1-\alpha'\right)\overline{\delta_N}}_{\text{fraction}} + \underbrace{\overline{\alpha}\delta'_S + (1-\overline{\alpha})\delta'_N}_{\text{end member}} + \underbrace{\alpha'\delta'_S + \left(1-\alpha'\right)\delta'_N}_{\text{nonlinear}} \quad (3)$$

175 where the bars denote the reference values during the LGM, the primes denote changes from the
176 LGM values, δ represents $\delta^{13}C$. We fix $\delta^{13}C_S$ and $\delta^{13}C_N$ at LGM to evaluate the water mass
177 fraction effect ($\delta^{13}C_{cons-frac}$), and fix α at LGM to evaluate the effect of changing end-member
178 value ($\delta^{13}C_{cons-end}$).

179 The difference between $\delta^{13}C_{cons}$ and $\delta^{13}C$ indicates the remineralization during the water
180 parcel transportation from its end-member region ($\delta^{13}C_{rem-path}$):

181 $$\delta^{13}C_{rem-path} = \delta^{13}C - \delta^{13}C_{cons} \quad (4).$$

182 The difference between the AOU based $\delta^{13}C_{rem}$ and the water mass mixing based $\delta^{13}C_{rem-path}$
183 indicates the remineralization in the end-member ($\delta^{13}C_{rem-end}$):

184 $$\delta^{13}C_{rem-end} = \delta^{13}C_{rem} - \delta^{13}C_{rem-path} \quad (5).$$

185 The remineralization in the end-member can also be estimated directly from the AOU based
186 $\delta^{13}C_{rem}$ in the end-member region, which shows similar anomalies as $\delta^{13}C_{rem-end}$ (Fig.S1). The
187 similar estimates of remineralization in the end-member validate our current decomposition
188 method.

189
190 2.3 Surface (physical) end-member and deep (paleo) end-member
191
192 In paleo applications, the end-member values are often estimated from the cores located in
193 the deep ocean near the source water regions (deep end-member) (e.g., Lund et al., 2015; Oppo et
194 al., 2015; Oppo and Fairbanks, 1987). Therefore, following the way of end-member estimation in
195 paleoceanography studies, the deep end-member in this study is estimated using the average over
196 50ºN-60ºN from 1,500m to 2,500m in the Atlantic for the NADW and south of 60ºS from 3,000m
197 to 4,000m in the Southern Ocean for the SSW in the model (illustrated in Figure 1 as boxes).
198 Physically, deep water is formed by deep convection from the surface. Hence, the end-
199 member values should be the values of the convected surface water, which will be referred to as
200 the surface end-member in this study. The surface end-member regions are the regions of deep
201 convection identified by the winter mixed layer depth in the model. Therefore, we define the
202 surface end-member of NADW as the average value over 50ºN-60ºN in the Atlantic at the bottom

of the euphotic zone (105m in the model) and the surface end-member of SSW as the average over the Southern Ocean (south of 60ºS, 60ºW-30ºE) at the bottom of the euphotic zone. The difference between the surface and deep end-member will be discussed in section 3.2. The surface end-member values are used in the $\delta^{13}C$ decomposition in this study.

3 Results and Discussion

3.1 Simulated deglacial Atlantic

From LGM to HS1, the simulated AMOC strength shows a large decrease, which is followed by the recovery during Bølling–Allerød (BA) (Figure. 2a). The simulated $^{231}Pa/^{230}Th$, a proxy for AMOC strength, agrees with the $^{231}Pa/^{230}Th$ reconstructions from the Bermuda Rise (McManus et al., 2004) (Figure. 2a), suggesting that C-iTRACE simulates a reasonable deglacial AMOC evolution.

The simulated mid-depth $\delta^{13}C$ shows a widespread decrease from the LGM to HS1 (Figure 1c). At the LGM, the high $\delta^{13}C$ associated with NADW penetrates southward at mid-depth (Figure 1a), and the simulated $\delta^{13}C$ north-south gradient in the Atlantic is in agreement with observations (Gu et al., 2020). Compared with the LGM, $\delta^{13}C$ at HS1 shows a decrease around 2,000m with the magnitude of the decrease largest in the North Atlantic and decreasing southward (Figure 1c). The average HS1 $\delta^{13}C$ decrease in the Atlantic at mid-depth is 1‰ in the model (Figure 2b). In the North Atlantic, simulated mid-depth $\delta^{13}C$ decreases by 1.0‰ above 2,000m, which agrees with observations (Figure 3a). However, the simulated $\delta^{13}C$ near 2,500m is much larger than the observations (Figure 1c), which might indicate an over-reduction of AMOC during HS1 in the model compared to reality. At the Brazil Margin, the simulated mid-depth $\delta^{13}C$ decreases by 0.5‰, consistent with the $\delta^{13}C$ changes in the observations (Figure 1c and Figure 3b). Despite the model-data mismatch near 2,500m in the North Atlantic, the simulated mid-depth $\delta^{13}C$ captures the major

feature in the observations, with a larger $\delta^{13}C$ decrease in the North Atlantic than the South Atlantic (Figure 1c) from LGM to HS1. Therefore, identifying the relative importance of different processes driving the mid-depth $\delta^{13}C$ decrease in the model context still has important implications for the real ocean.

To assess the causes of the mid-depth $\delta^{13}C$ decrease in the model, we first evaluate whether the mechanisms proposed previously are consistent with our simulation: i) a greater fraction of SSW, ii) reduced ventilation and enhanced remineralization, and iii) a decrease in the NADW deep end-member value. Indeed, with the weakening of AMOC, there is almost no deep convection in the North Atlantic and the production of NADW is greatly reduced at HS1, with significantly more SSW and less NADW at the mid-depth (Figure 1 d-f). The average proportion of SSW (indicated by Dye-South) increases by 30% in the mid-depth Atlantic (Figure 2c). Although greatly reduced compared with LGM, the NADW water mass fraction is still ~50% in the mid-depth Atlantic during HS1 because AMOC is not fully collapsed (~4Sv). With less young NADW ventilating the mid-depth Atlantic at HS1, the water age increases in the mid-depth Atlantic during HS1, allowing more remineralized material to accumulate, with the largest increase found near 2-3 km between 30-60 ºN (Figure 1g-i). The average ideal age increases by 900 years, and the idealized ventilation age increases by 1,200 years (Figure 2d). In our simulation, the deep $\delta^{13}C$ end-member is relatively stable for SSW, with a slight decrease from the LGM (0.19‰) to HS1 (-0.17‰), consistent with the small difference found in observations between LGM and HS1 (Oppo et al. 2015). However, the NADW deep end-member value changes dramatically (Figure 2e) from 1.32‰ in the LGM to -0.06‰ in HS1 (Table 1). This 1.38‰ difference is similar to the observational estimate of 1.01‰ (1.51‰ in LGM and 0.5‰ in HS1) in Oppo et al. (2015). Therefore,

qualitatively, the simulation suggests that all the proposed mechanisms have the potential to reduce HS1 $\delta^{13}C$ in the model.

3.2 Surface and deep end-member changes

Surface and deep end-member $\delta^{13}C$ values show similar evolutions during the last deglaciation. For both SSW and NADW, deep end-member values are always lower than the surface end-members because both water masses get less ventilated with depth (as indicated by increasing water age with depth; Figure 1g and h), which leads to accumulation of low $\delta^{13}C$ respired carbon at depth. For SSW, both surface and deep end-member values are stable (Figure 4a and Table 1). But for NADW, surface and deep end-members decrease during HS1, with stronger decrease in the deep end-member.

The surface NADW end-member $\delta^{13}C$ decrease at the bottom of the euphotic zone is associated with the decrease of $\delta^{13}C_{rem}$ and the $\delta^{13}C$ decrease in the atmospheric CO_2 (Figure 4b). The $\delta^{13}C_{rem}$ in the NADW surface end-member mimics the change of the AMOC, as it starts to decrease at 19ka and almost reaches the minimum at 17ka, following the evolution of the ventilation age (Figure S2a and c). Early in the deglaciation, the prescribed $\delta^{13}C$ in the atmospheric CO_2 increases slightly by 0.05‰ at 17.5ka, leading to an increase of $\delta^{13}C_{pre}$ in the North Atlantic surface water due to air-sea gas exchange (Figure 4b). This $\delta^{13}C_{pre}$ increase compensates the $\delta^{13}C_{rem}$ decrease, leading to a quite small decrease of the $\delta^{13}C$ NADW surface end-member during the early deglaciation. After 17.5ka, when the $\delta^{13}C$ in the atmospheric CO_2 begins to decrease, the $\delta^{13}C_{pre}$ decreases, which accelerates the $\delta^{13}C$ surface end-member decrease. The 0.78‰ HS1 $\delta^{13}C$ decrease in the NADW surface end-member incorporates 0.28‰ decrease in the

271 $\delta^{13}C_{pre}$ related to the $\delta^{13}C$ decrease in atmospheric CO_2 and 0.5‰ decrease in $\delta^{13}C_{rem}$ probably
272 related to increased ventilation age due to AMOC slow down.

273 The NADW surface end-member change influences the NADW deep end-member value
274 (Figure 4c). From LGM to HS1, the SSW% in the NADW deep end-member region increases by
275 ~30%, and combined with the $\delta^{13}C$ decrease in the NADW surface end-member value, contributes
276 to 0.86‰ of the $\delta^{13}C$ decrease in $\delta^{13}C_{cons}$, which is 62% of the total $\delta^{13}C$ decrease in the NADW
277 deep end-member. In $\delta^{13}C_{cons}$, the decrease of the $\delta^{13}C$ surface end-member is much more
278 important than the increased amount of SSW (Figure 4c). If there were no surface end-member
279 change, changes in water mass fraction alone would decrease $\delta^{13}C$ by only 0.31‰ ($\delta^{13}C_{cons-frac}$).
280 In contrast, if there were no changes in water mass fraction, the NADW surface end-member
281 decrease would cause a $\delta^{13}C$ decrease of 0.76‰ ($\delta^{13}C_{cons-end}$), more than twice the effect of
282 $\delta^{13}C_{cons-frac}$. It is noteworthy that the nonlinear term in Eq. 3 is -0.21‰, which is not negligible.
283 But the existence of this term does not affect our conclusions on the relative contributions of the
284 other two terms.

285 We find that accumulated remineralized $\delta^{13}C$ is the most important factor causing the
286 deglacial deep NADW end-member decrease. The total $\delta^{13}C_{rem}$ anomaly in the NADW deep end-
287 member has a similar magnitude of changes as the $\delta^{13}C$ anomaly, suggesting a dominant role of
288 remineralization (Figure 4d). The evolution of the $\delta^{13}C_{rem}$ in the NADW deep end-member shows
289 a similar evolution as the idealized water age tracers (Figure S2b and d), further suggesting that
290 the deep NADW end-member change during HS1 is mainly due to the accumulation of respired
291 carbon caused by reduced ventilation that accompanies the weak AMOC.

292 This $\delta^{13}C_{rem}$ includes the $\delta^{13}C_{rem}$ in the NADW surface end-member ($\delta^{13}C_{rem-end}$) at
293 the bottom of the euphotic zone, and that added as water sinks from the near-surface to the NADW

deep end-member region ($\delta^{13}C_{rem-path}$), which show different evolutions during the deglaciation as discussed below. Since the SSW $\delta^{13}C$ end-member, including $\delta^{13}C_{rem}$ in SSW, is relatively stable, and the change of water mass composition plays a minor role in the $\delta^{13}C$ change, we consider the $\delta^{13}C_{rem-end}$ is mostly from the change in NADW. The evolution of the estimated $\delta^{13}C_{rem-end}$ agrees with that of the $\delta^{13}C_{rem}$ in the NADW surface end-member (Figure 4b purple and 4d navy; Figure S1a), both of which show a rapid decrease starting at 18ka and reaching stable values at 17ka. The $\delta^{13}C_{rem-path}$, however, shows a more gradual decrease that continues until the end of HS1, indicating increasingly greater accumulation of respired carbon at depth as the AMOC shutdown continues. The 1.21‰ decrease in $\delta^{13}C_{rem}$ from LGM to HS1 is the most crucial factor in the $\delta^{13}C$ NADW deep end-member decrease, which incorporates almost similar contributions from $\delta^{13}C_{rem-end}$ and $\delta^{13}C_{rem-path}$(Figure 4d). The initial decrease of $\delta^{13}C_{rem}$ is mainly due to $\delta^{13}C_{rem-end}$, with $\delta^{13}C_{rem-path}$ increasingly important from 17ka to 15ka (Figure 4e).

The comparison of the surface end-member and the deep end-member in the Atlantic suggests that because the change of $\delta^{13}C_{rem-path}$ is not negligible, the deep NADW end-member incorporates additional remineralization from the surface end-member. Therefore, it is more appropriate to use the surface end-member to diagnose the $\delta^{13}C$ change in the Atlantic. However, the surface and deep end-members are probably interdependent. During HS1, the productivity in the NADW formation region is significantly lower than that during the LGM. Therefore, more remineralized material in the NADW surface end-member is due to changes in the physical processes, rather than due to local biological processes. The accumulated remineralized material in the NADW surface end-member agrees with the increased ventilation age in the NADW surface

316 end-member (Figure S2c), which is likely due to the mixing with water at depth with accumulated
317 remineralized material and older water age.
318 A recent study suggests that the deglacial surface and mid-depth change could also be
319 influenced by air-sea gas exchange (Lynch-Stieglitz et al., 2019). In our model, the air-sea gas
320 exchange effect is incorporated in $\delta^{13}C_{pre}$, which is not as important as $\delta^{13}C_{rem}$ in the surface
321 North Atlantic (Figure 4b). This case is especially true in the mid-depth Atlantic (Figure 5 and
322 Figure 6b). Therefore, the air-sea gas exchange plays a minor role in the deglacial Atlantic $\delta^{13}C$
323 change in our model.
324
325 3.3 Decomposition of the Atlantic mid-depth $\delta^{13}C$ decrease
326 The results of the quantitative decomposition of the deep NADW end-member $\delta^{13}C$ also
327 apply to the mid-depth Atlantic. The combined contribution from the water mass fraction and end-
328 member ($\delta^{13}C_{cons}$) accounts for 70% of the total $\delta^{13}C$ decrease in the model (Figure 5b and 6a),
329 among which the effect of end-member change ($\delta^{13}C_{cons-end}$) is much more important than the
330 water mass composition ($\delta^{13}C_{cons-frac}$). Therefore, our results suggest that although SSW
331 increases by 30% in the mid-depth Atlantic, the prevailing explanation of the mid-depth
332 $\delta^{13}C$ decrease due to the increase of SSW (e.g., Boyle & Keigwin, 1987; Keigwin & Lehman,
333 1994; Sarnthein et al., 1994) is probably not as important as once assumed.
334 The remineralization associated with the AMOC induced ventilation change accounts for
335 the majority of the $\delta^{13}C$ change during the last deglaciation. The $\delta^{13}C_{rem}$ change between HS1
336 and LGM is similar to the $\delta^{13}C$ change in both pattern and magnitude (Figure 5d and 6b). The
337 $\delta^{13}C_{rem}$ change (Figure 5d) is negatively correlated with the ventilation change in the Atlantic
338 (Figure 1i), with the region having a larger increase in the ventilation age showing larger $\delta^{13}C_{rem}$

339 decrease, and vice versa. When the AMOC is weakened, the mid-depth Atlantic ventilation age
340 increases, and the accumulation of the respired organic carbon causes the decrease in $\delta^{13}C_{rem}$.
341 Similar to the NADW deep end-member, during the early deglaciation (19ka-17ka), the
342 $\delta^{13}C_{rem}$ decrease in the mid-depth Atlantic is caused almost solely by remineralization in the end-
343 member ($\delta^{13}C_{rem-end}$) rather than along the NADW transport pathway ($\delta^{13}C_{rem-path}$). After
344 17ka, when the simulated AMOC is greatly weakened, remineralized carbon along the pathway
345 gradually increases (Figure 6b). The $\delta^{13}C_{rem-end}$ accounts for about 70% of the $\delta^{13}C_{rem}$ change
346 from LGM to HS1, while the $\delta^{13}C_{rem-path}$ accounts for about 30%, suggesting that the
347 $\delta^{13}C_{rem}$ in the NADW surface end-member is the critical factor for the deglacial $\delta^{13}C_{rem}$ change.
348 During HS1, simulated $\delta^{13}C$ keeps decreasing in the mid-depth Atlantic (Figure 6), as well as in
349 the Brazil Margin (Figure 3b). This decreasing trend is mainly due to $\delta^{13}C_{rem-path}$ (Figure 6b),
350 which might suggest that the simulated AMOC is too weak for too long during HS1. From HS1 to
351 the Bølling–Allerød (BA), with the abrupt recovery of the AMOC, the simulated $\delta^{13}C$ also
352 increases abruptly (Figure 3 and Figure 6) due to the abrupt increase in $\delta^{13}C_{rem-end}$ (Figure 6b).
353 This simulated abrupt mid-depth $\delta^{13}C$ change during the HS1-BA transition is not recorded in the
354 mid-depth $\delta^{13}C$ observations (Figure 3), probably because the resolutions of these observations
355 are not high enough to resolve such abrupt changes, or because the model has deficiency in
356 representing the physical environments and tracer fields, which remains to be explored in the future.
357 Our results are in agreement with recent studies (Lacerra et al., 2017; Schmittner and Lund,
358 2015; Voigt et al., 2017) showing that greater remineralization caused by ocean circulation change
359 is the main reason for the $\delta^{13}C$ decrease in the mid-depth Atlantic. However, unlike these studies,
360 our results further suggest that it is the remineralized materials presented in the near-surface North
361 Atlantic waters, rather than the addition of remineralization along the pathway from the surface

362 to the deep ocean, that contributes more to the $\delta^{13}C$ decrease at mid-depths, especially during the
363 early stage of the deglaciation. From the LGM to HS1, the accumulation of the respired carbon in
364 the mid-depth leads to the DIC increase in the simulation (Figure 7), which agrees with the
365 observational estimates from the Brazil Margin B/Ca records (Lacerra et al., 2017), supporting the
366 hypothesis that the mid-depth Atlantic sequestered a significant amount of carbon, muting the
367 atmospheric CO_2 increase during HS1 (Lacerra et al., 2017). Interestingly, the intermediate depth
368 DIC shows a decrease during the deglaciation (Figure 7c), also consistent with B/Ca records
369 (Lacerra et al., 2019). At the same time, intermediate depth $\delta^{13}C$ increases, mainly caused by
370 $\delta^{13}C_{rem-path}$ (Figure 5), suggesting reduced remineralization in the intermediate depth (Lacerra
371 et al., 2019). The opposite changes between the intermediate depth and mid-depth suggesting
372 different roles of Antarctic Intermediate Water (AAIW) and NADW in the deglacial atmospheric
373 CO_2 rise and warrant further investigation.
374
375 **4. Conclusions**
376 We present a quantitative examination of previously proposed mechanisms for the Atlantic
377 deglacial mid-depth $\delta^{13}C$ decrease in a transient simulation. Our modeling results suggest that
378 although SSW fraction increases in the mid-depth Atlantic, change of the water mass composition
379 alone plays a minor role in the mid-depth $\delta^{13}C$ decrease. Instead, the accumulation of the respired
380 carbon resulting from the reduced ventilation associated with AMOC is the dominant cause of the
381 deglacial mid-depth $\delta^{13}C$ decrease. Furthermore, our results suggest that remineralization in the
382 NADW near-surface end-member is more important than the remineralization during the NADW
383 transport pathway. During HS1, with the weak AMOC, the near-surface water from the NADW
384 formation region shows reduced ventilation, favoring the accumulation of the remineralized

materials. In previous studies (e.g., Lund et al., 2015; Oppo et al., 2015; Oppo and Fairbanks, 1987), the deep end-member, where deep ocean $\delta^{13}C$ records come from, was used to quantify the $\delta^{13}C$ change in the Atlantic. Our results suggest that the deep NADW end-member includes additional remineralization from the surface end-member, and the surface end-member is not only more appropriate for diagnosing the mechanism of $\delta^{13}C$ changes, but also reveals a significant process contributing to the $\delta^{13}C$ change, especially during the early deglaciation. However, the surface and deep NADW end-members could be interdependent, and the increased remineralized material in the surface NADW end-member during HS1 likely also reflects mixing with older water at depth under a weak but not fully collapsed AMOC. Last but not least, this study presents a diagnosis of the $\delta^{13}C$ change by estimating each component, which can be further improved in accuracy with more sophisticated models explicitly simulating different components in the model in the future.

Acknowledgments

This work is supported by US National Science Foundation (NSF) P2C2 projects (1401778, 1401802, and 1566432), and the National Science Foundation of China No. 41630527. S.G. is supported by Shanghai Pujiang program. We would like to acknowledge high-performance computing support from Yellowstone (ark:/85065/d7wd3xhc) and Cheyenne (doi:10.5065/D6RX99HX) provided by NCAR's Computational and Information Systems Laboratory and by the Center for High Performance Computing and System Simulation, Pilot National Laboratory for Marine Science and Technology (Qingdao). Data used to produce the results in this study can be obtained from the NCAR Campaign Storage: /glade/campaign/univ/ucub0050/sifan/Atl_mid_d13C or by contacting the authors.

Reference

Bauska, T.K., Baggenstos, D., Brook, E.J., Mix, A.C., Marcott, S.A., Petrenko, V. V, Schaefer, H., Severinghaus, J.P., Lee, J.E., 2016. Carbon isotopes characterize rapid changes in atmospheric carbon dioxide during the last deglaciation. Proc. Natl. Acad. Sci. U. S. A. 113, 3465–3470. https://doi.org/10.1073/pnas.1513868113

Boyle, E.A., Keigwin, L., 1987. North Atlantic thermohaline circulation during the past 20,000 years linked to high-latitude surface temperature. Nature. https://doi.org/10.1038/330035a0

Broecker, W.S., Maier-Reimer, E., 1992. The influence of air and sea exchange on the carbon isotope distribution in the sea. Global Biogeochem. Cycles 6, 315–320.

Curry, W.B., Oppo, D.W., 2005. Glacial water mass geometry and the distribution of δ13 C of ΣCO2 in the western Atlantic Ocean. Paleoceanography 20.

Danabasoglu, G., Bates, S.C., Briegleb, B.P., Jayne, S.R., Jochum, M., Large, W.G., Peacock, S., Yeager, S.G., 2012. The CCSM4 ocean component. J. Clim. 25, 1361–1389. https://doi.org/10.1175/JCLI-D-11-00091.1

Dokken, T.M., Jansen, E., 1999. Rapid changes in the mechanism of ocean convection during the last glacial period. Nature 401, 458–461. https://doi.org/10.1038/46753

Gherardi, J.-M., Labeyrie, L., Nave, S., Francois, R., McManus, J.F., Cortijo, E., 2009. Glacial-interglacial circulation changes inferred from 231 Pa/ 230 Th sedimentary record in the North Atlantic region. Paleoceanography 24, PA2204. https://doi.org/10.1029/2008PA001696

Gu, S., Liu, Z., 2017. 231Pa and 230Th in the ocean model of the Community Earth System Model (CESM1.3). Geosci. Model Dev. 10, 4723–4742. https://doi.org/10.5194/gmd-10-4723-2017

Gu, S., Liu, Z., Lynch- Stieglitz, J., Jahn, A., Zhang, J., Lindsay, K., Wu, L., 2019. Assessing the Ability of Zonal d18O Contrast in Benthic Foraminifera to Reconstruct Deglacial Evolution of Atlantic Meridional Overturning Circulation. Paleoceanogr. Paleoclimatology 34, 800–812. https://doi.org/10.1029/2019PA003564

Gu, S., Liu, Z., Oppo, D.W., Lynch-Stieglitz, J., Jahn, A., Zhang, J., Wu, L., 2020. Assessing the potential capability of reconstructing glacial Atlantic water masses and AMOC using multiple proxies in CESM. Earth Planet. Sci. Lett. 541, 116294. https://doi.org/10.1016/j.epsl.2020.116294

Gu, S., Liu, Z., Zhang, J., Rempfer, J., Joos, F., Oppo, D.W., 2017. Coherent response of Antarctic Intermediate Water and Atlantic Meridional Overturning Circulation during the last deglaciation: reconciling contrasting neodymium isotope reconstructions from the tropical Atlantic. Paleoceanography 32, 1036–1053. https://doi.org/10.1002/2017PA003092

He, F., 2011. SIMULATING TRANSIENT CLIMATE EVOLUTION OF THE LAST DEGLACIATION WITH CCSM3.

Howe, J.N.W., Piotrowski, A.M., Noble, T.L., Mulitza, S., Chiessi, C.M., Bayon, G., 2016. North Atlantic Deep Water Production during the Last Glacial Maximum. Nat. Commun. 7, 11765. https://doi.org/10.1038/ncomms11765

Jahn, A., Lindsay, K., Giraud, X., Gruber, N., Otto-Bliesner, B.L., Liu, Z., Brady, E.C., 2015. Carbon isotopes in the ocean model of the Community Earth System Model (CESM1). Geosci. Model Dev. 8, 2419–2434. https://doi.org/10.5194/gmd-8-2419-2015

Joos, F., Spahni, R., 2008. Rates of change in natural and anthropogenic radiative forcing over the past 20,000 years. Proc. Natl. Acad. Sci. U. S. A. 105, 1425–1430. https://doi.org/10.1073/pnas.0707386105

Keigwin, L.D., Lehman, S.J., 1994. Deep circulation change linked to HEINRICH Event 1 and Younger Dryas in a middepth North Atlantic Core. Paleoceanography 9, 185–194. https://doi.org/10.1029/94PA00032

Khatiwala, S., Schmittner, A., Muglia, J., 2019. Air-sea disequilibrium enhances ocean carbon storage during glacial periods. Sci. Adv.

Lacerra, M., Lund, D., Yu, J., Schmittner, A., 2017. Carbon storage in the mid-depth Atlantic during millennial-scale climate events. Paleoceanography 32, 780–795. https://doi.org/10.1002/2016PA003081

Lacerra, M., Lund, D.C., Gebbie, G., Oppo, D.W., Yu, J., Schmittner, A., Umling, N.E., 2019. Less remineralized carbon in the intermediate depth South Atlantic during Heinrich Stadial 1. Paleoceanogr. Paleoclimatology 34, 1218–1233. https://doi.org/10.1029/2018PA003537

Liu, Z., Otto-Bliesner, B.L., He, F., Brady, E.C., Tomas, R., Clark, P.U., Carlson, a E., Lynch-Stieglitz, J., Curry, W., Brook, E., Erickson, D., Jacob, R., Kutzbach, J., Cheng, J., 2009. Transient simulation of last deglaciation with a new mechanism for Bolling-Allerod warming. Science (80-.). 325, 310–314. https://doi.org/10.1126/science.1171041

Lund, D.C., Tessin, A.C., Hoffman, J.L., Schmittner, A., 2015. Southwest Atlantic water mass evolution during the last deglaciation. Paleoceanogr. Paleoclimatology 477–494. https://doi.org/10.1002/2014PA002657.Received

Lynch-Stieglitz, J., Fairbanks, R.G., 1994. A Conservative Tracer for Glacial Ocean Circulation from Carbon-Isotope and Palaeo-Nutrient Measurements in Benthic Foraminifera. Nature 369, 308–310.

Lynch-Stieglitz, J., Valley, S.G., Schmidt, M.W., 2019. Temperature-dependent ocean–atmosphere equilibration of carbon isotopes in surface and intermediate waters over the deglaciation. Earth Planet. Sci. Lett. 506, 466–475. https://doi.org/10.1016/j.epsl.2018.11.024

Mahowald, N.M., Muhs, D.R., Levis, S., Rasch, P.J., Yoshioka, M., Zender, C.S., Luo, C., 2006. Change in atmospheric mineral aerosols in response to climate: Last glacial period, preindustrial, modern, and doubled carbon dioxide climates. J. Geophys. Res. Atmos. 111. https://doi.org/10.1029/2005JD006653

McManus, J., Francois, R., Gherardi, J., 2004. Collapse and rapid resumption of Atlantic meridional circulation linked to deglacial climate changes. Nature 428, 834–837.

Oppo, D.W., Curry, W.B., McManus, J.F., 2015. What do benthic δ13C and δ18O data tell us about Atlantic circulation during Heinrich Stadial 1? Paleoceanography 30, 353–368. https://doi.org/10.1002/2014PA002667

Oppo, D.W., Fairbanks, R.G., 1987. Variability in the deep and intermediate water circulation of the Atlantic Ocean during the past 25,000 years: Northern Hemisphere modulation of the Southern Ocean. Earth Planet. Sci. Lett. 86, 1–15. https://doi.org/10.1016/0012-821X(87)90183-X

Piotrowski, A.M., Goldstein, S.L., Hemming, S.R., Fairbanks, R.G., 2005. Temporal relationship of carbon cycling and ocean circulation at glacial boundaries. Science (80-.). 307, 1933–1938. https://doi.org/10.1126/science.1104883

Rickaby, R.E.M., Elderfield, H., 2005. Evidence from the high-latitude North Atlantic for variations in Antarctic Intermediate water flow during the last deglaciation. Geochemistry, Geophys. Geosystems 6. https://doi.org/10.1029/2004GC000858

Sarmiento, J.L., Gruber, N., 1996. Ocean Biogeochemical Dynamics.

Sarnthein, M., Winn, K., Jung, S.J.A., Duplessy, J. - C, Labeyrie, L., Erlenkeuser, H., Ganssen,

G., 1994. Changes in East Atlantic Deepwater Circulation over the last 30,000 years: Eight time slice reconstructions. Paleoceanography 9, 209–267. https://doi.org/10.1029/93PA03301

Schmitt, J., Schneider, R., Elsig, J., Leuenberger, D., Lourantou, a., Chappellaz, J., Kohler, P., Joos, F., Stocker, T.F., Leuenberger, M., Fischer, H., 2012. Carbon Isotope Constraints on the Deglacial CO2 Rise from Ice Cores. Science (80-.). 336, 711–714. https://doi.org/10.1126/science.1217161

Schmittner, A., Lund, D.C., 2015. Early deglacial Atlantic overturning decline and its role in atmospheric CO2 rise inferred from carbon isotopes (δ13C). Clim. Past 11, 135–152. https://doi.org/10.5194/cp-11-135-2015

Shakun, J.D., Clark, P.U., He, F., Marcott, S. a, Mix, A.C., Liu, Z., Otto-Bliesner, B., Schmittner, A., Bard, E., 2012. Global warming preceded by increasing carbon dioxide concentrations during the last deglaciation. Nature 484, 49–54. https://doi.org/10.1038/nature10915

Tessin, A.C., Lund, D.C., 2013. Isotopically depleted carbon in the mid-depth South Atlantic during the last deglaciation. Paleoceanography 28, 296–306. https://doi.org/10.1002/palo.20026

Thornalley, D.J.R., Elderfield, H., McCave, I.N., 2010. Intermediate and deep water paleoceanography of the northern North Atlantic over the past 21,000 years. Paleoceanography 25, PA1211. https://doi.org/10.1029/2009PA001833

Voigt, I., Cruz, A.P.S., Mulitza, S., Chiessi, C.M., Mackensen, A., Lippold, J., 2017. Variability in mid-depth ventilation of the western Atlantic Ocean during the last deglaciation. Palaeogeography 32, 1–27. https://doi.org/10.1002/2017PA003095

Waelbroeck, C., Skinner, L.C., Labeyrie, L., Duplessy, J.C., Michel, E., Vazquez Riveiros, N., Gherardi, J.M., Dewilde, F., 2011. The timing of deglacial circulation changes in the Atlantic. Paleoceanography 26. https://doi.org/10.1029/2010PA002007

Zahn, R., Schönfeld, J., Kudrass, H.R., Park, M.H., Erlenkeuser, H., Grootes, P., 1997. Thermohaline instability in the North Atlantic during melt water events: Stable isotope and ice-rafted detritus records from core SO75-26KL, Portuguese margin. Paleoceanography 12, 696–710. https://doi.org/10.1029/97PA00581

Zhang, J., 2016. Understanding the deglacial evolution of deep Atlantic water masses in an isotope-enabled ocean model.

Zhang, J., Liu, Z., Brady, E.C., Jahn, A., Oppo, D.W., Clark, P.U., Marcott, S.A., Lindsay, K., 2017. Asynchronous warming and oxygen isotope evolution of deep Atlantic water masses during the last deglaciation. Proc. Natl. Acad. Sci. 114, 11075–11080. https://doi.org/10.1073/pnas.1704512114

Tables 1. $\delta^{13}C$ deep end-member and surface end-member values at LGM and HS1 in the model.

Deep end-member			**Surface end-member**		
	NADW	AABW		NADW	AABW
LGM	1.32‰	0.19‰	LGM	1.72‰	0.51‰
HS1	-0.06‰	-0.17‰	HS1	0.94‰	0.53‰

Figures:

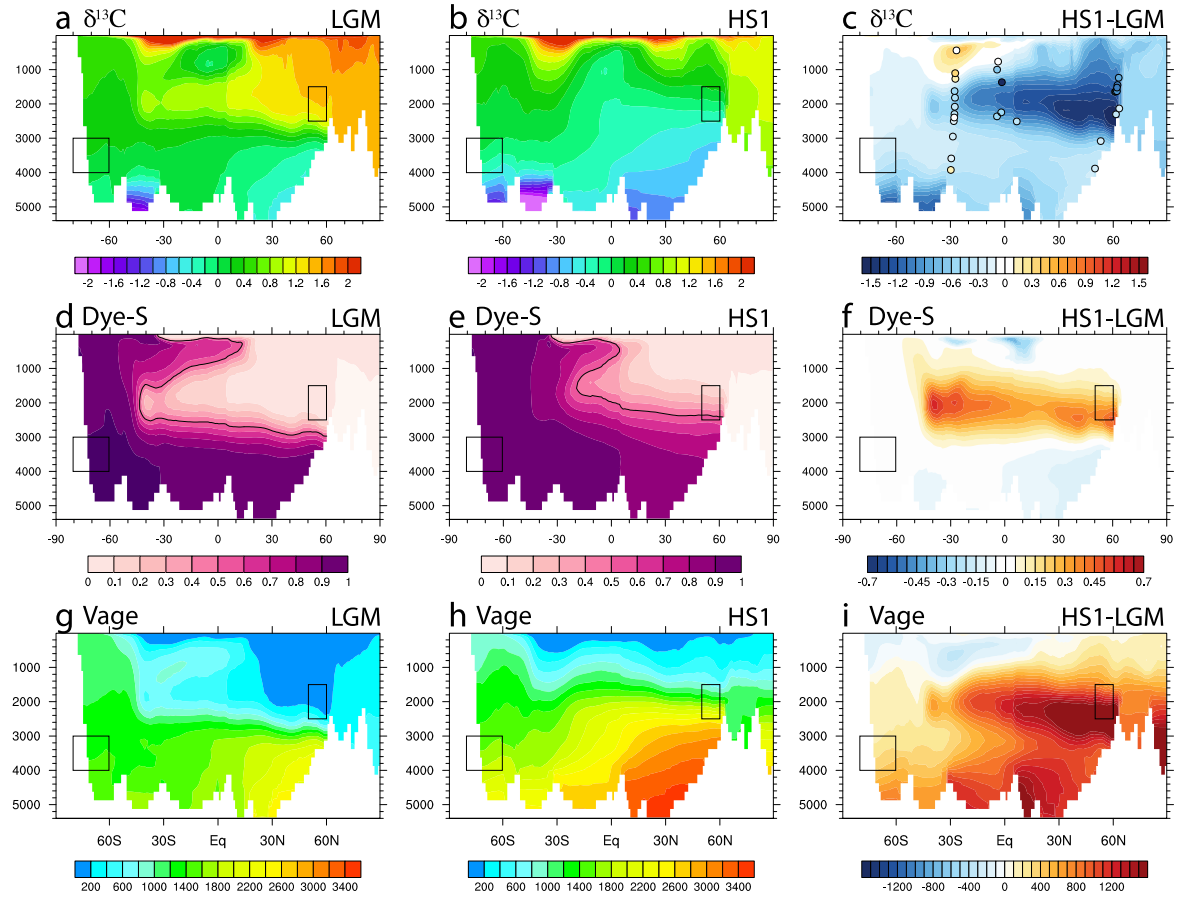

Figure 1. Atlantic zonal mean distributions at LGM (left), HS1 (center), and the difference between HS1 and LGM (right). (a-c) $\delta^{13}C$; (d-f) Dye-South; (g-i) idealized ventilation age. The locations of deep end-member are indicated by the boxes. The observational $\delta^{13}C$ HS1-LGM difference (listed in Table S1) are overlaid as colored circles in c.

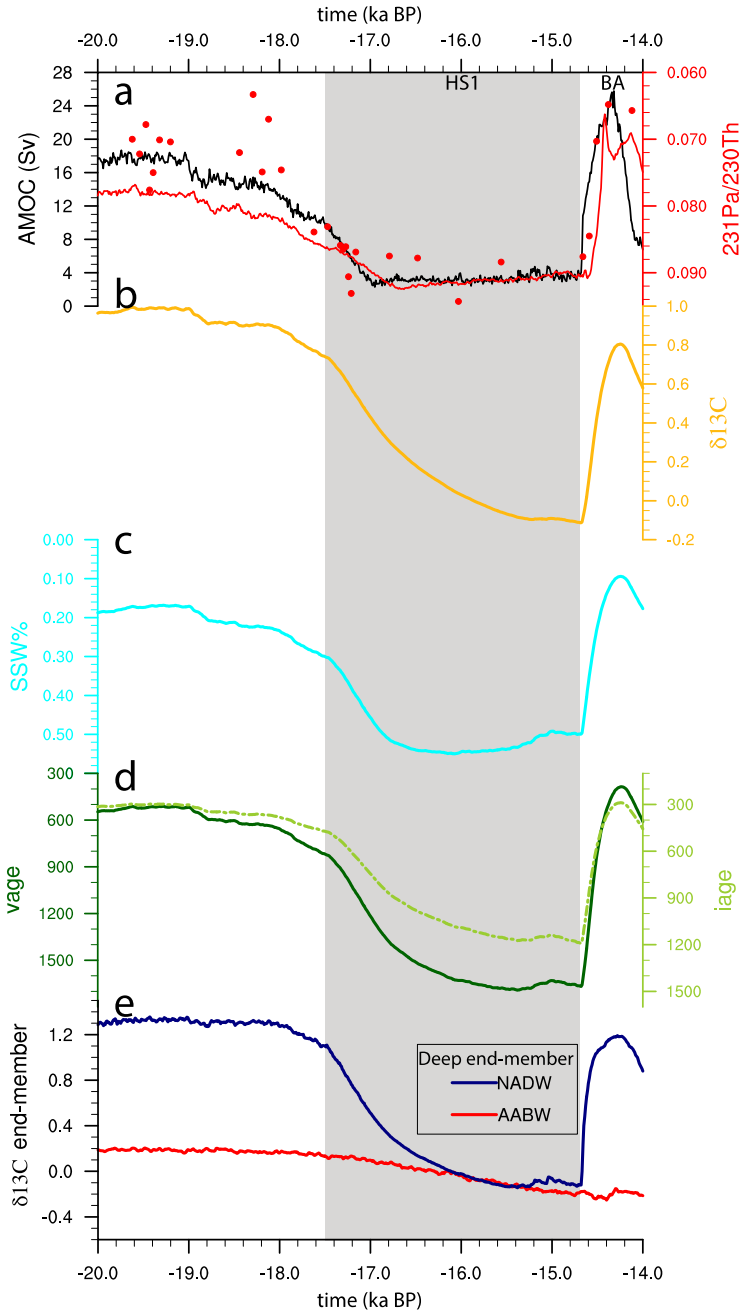

Figure 2. Simulated Atlantic evolution in C-iTRACE. (a) AMOC strength (black) and simulated $^{231}Pa/^{230}Th$ (red curve) and $^{231}Pa/^{230}Th$ observations (red dots) at the site OCE326-GGC5 (33°43'N, 57°35'W, 4.55km). (b) Atlantic mid-depth average $\delta^{13}C$ evolution. (c) Atlantic mid-depth average SSW percentage. (d) Atlantic mid-depth average ideal age (dashed light green) and idealized ventilation age (solid dark green). (e) $\delta^{13}C$ deep end-member values for NADW (navy) and AABW (red). Here Atlantic mid-depth average is calculated by averaging from 1,500m to 2,500m.

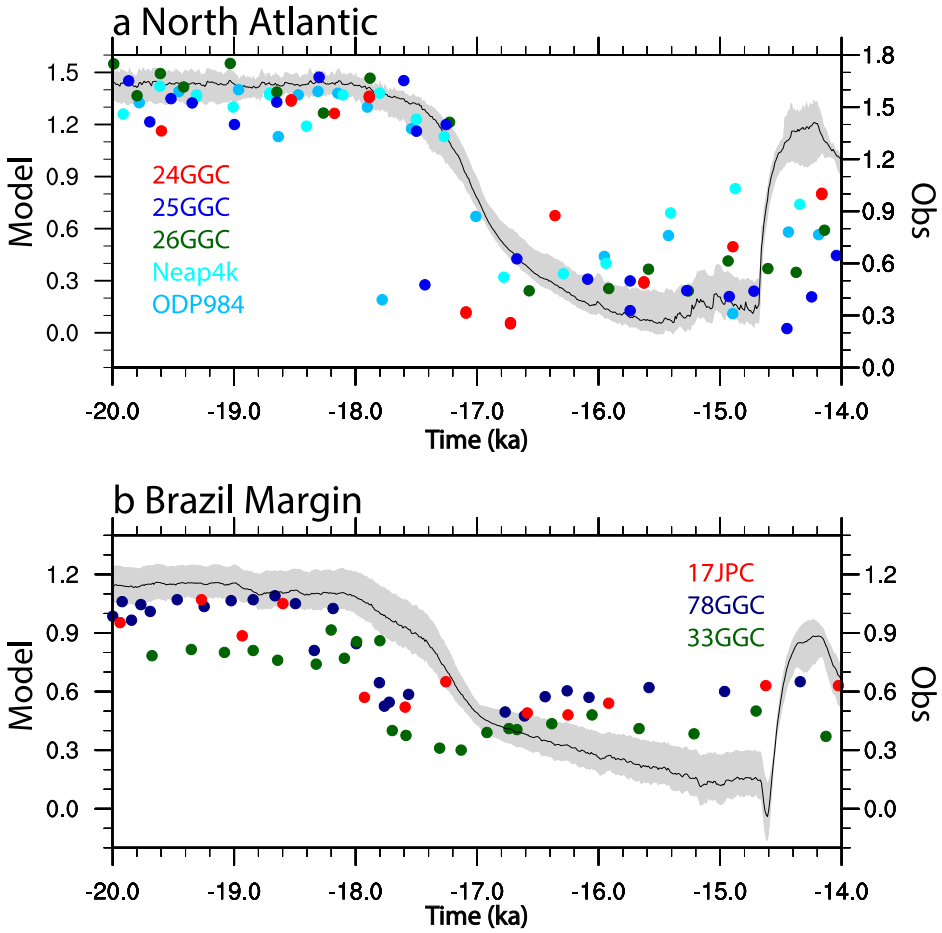

Figure 3. Model data comparison of deglacial mid-depth $\delta^{13}C$ evolution. (a) North Atlantic: model averaged over 55°N-60°N, 1500m-1700m according to the available observations. (b) Brazil Margin: model averaged over 25°S-30°S, 40°W-50°W, 1600m-2100m according the available observations. Grey shading is the model spread in each region. Details of each observational site are listed in table S1.

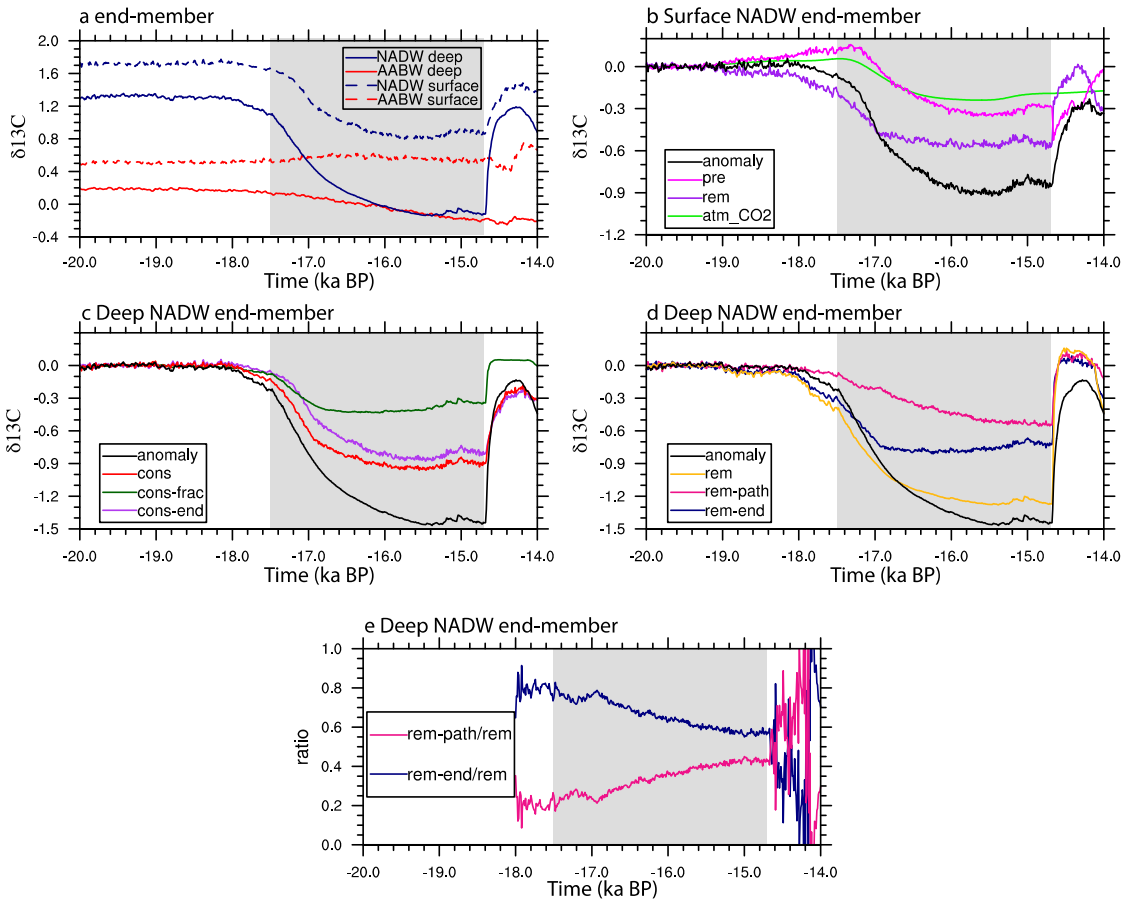

Figure 4. Evolution and decomposition of surface and deep end-member. (a) Surface end-member (dash) and deep end-member (solid) evolutions for NADW (navy) and SSW (red). (b) NADW $\delta^{13}C$ surface end-member anomaly (black), preformed $\delta^{13}C$ anomaly in NADW surface end-member (magenta), remineralized $\delta^{13}C$ anomaly in NADW surface end-member (purple), and $\delta^{13}C$ anomaly in atmospheric CO_2 from Schmitt et al. (2012) (green). (c) NADW deep end-member $\delta^{13}C$ anomaly (black), $\delta^{13}C_{cons}$ anomaly (red), $\delta^{13}C_{cons-frac}$ anomaly (green), and $\delta^{13}C_{cons-end}$ anomaly (purple). (d) NADW deep end-member $\delta^{13}C$ anomaly (black), $\delta^{13}C_{rem}$ in NADW deep end-member (yellow), $\delta^{13}C_{rem-path}$ anomaly in NADW deep end-member (pink), estimated remineralized anomaly in NADW surface end-member ($\delta^{13}C_{rem-end}$) from ($\delta^{13}C_{rem} - \delta^{13}C_{rem-path}$) (navy). (e) ratio of $\delta^{13}C_{rem-path}/\delta^{13}C_{rem}$ (pink) and $\delta^{13}C_{rem-end}/\delta^{13}C_{rem}$ (navy).

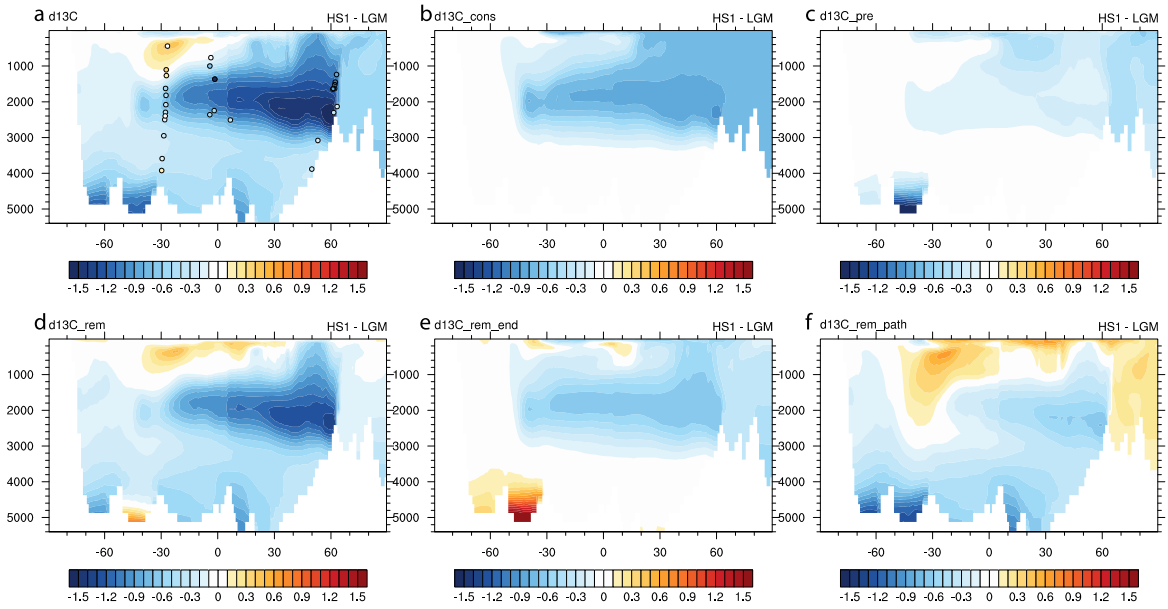

Figure 5. Decomposed $\delta^{13}C$ Atlantic zonal mean difference between HS1 and LGM. (a) $\delta^{13}C$ (b) $\delta^{13}C_{cons}$, (c) $\delta^{13}C_{pre}$, (d) $\delta^{13}C_{rem}$, (e) $\delta^{13}C_{rem-end}$ ($\delta^{13}C_{rem} - \delta^{13}C_{rem-path}$), (f) $\delta^{13}C_{rem-path}$.

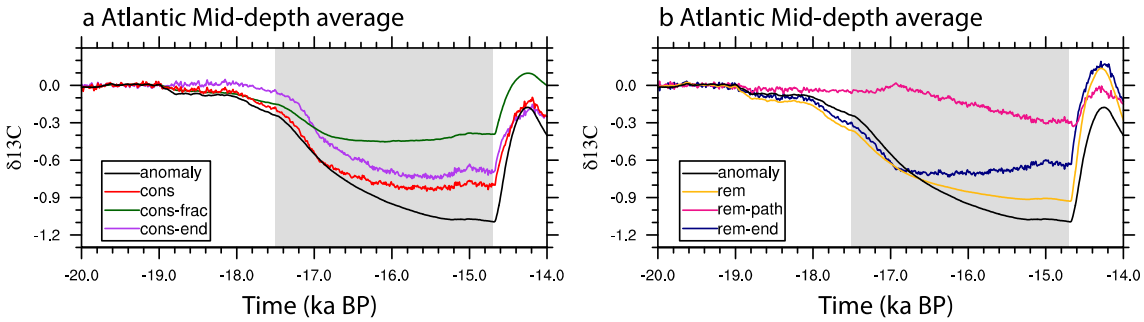

Figure 6. Decomposition of Atlantic mid-depth (1500m-2500m) average $\delta^{13}C$. (a) $\delta^{13}C$ anomaly (black), $\delta^{13}C_{cons}$ anomaly (red), $\delta^{13}C_{cons-frac}$ anomaly (green), and $\delta^{13}C_{cons-end}$ anomaly (purple). (b) $\delta^{13}C$ anomaly (black), $\delta^{13}C_{rem}$ anomaly (yellow), $\delta^{13}C_{rem-path}$ anomaly (pink), $\delta^{13}C_{rem-end}$ anomaly estimated from $\delta^{13}C_{rem} - \delta^{13}C_{rem-path}$ (navy).

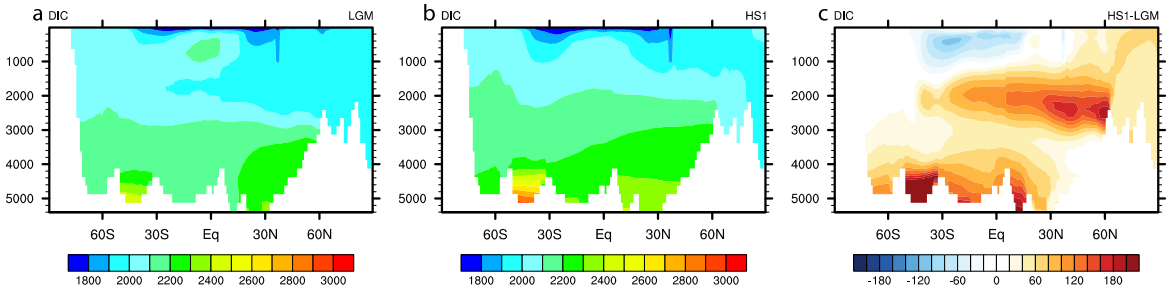

Figure 7. Simulate DIC concentration normalized by salinity at LGM (a), HS1 (b), and the difference between HS1 and LGM (c) (unit in μmol/kg).

Supplementary Materials for "**Remineralization dominating the $\delta^{13}C$ decrease in the mid-depth Atlantic during the last deglaciation**"

Sifan Gu[1,2], Zhengyu Liu[3], Delia W. Oppo[4], Jean Lynch-Stieglitz[5], Alexandra Jahn[6], Jiaxu Zhang[7], Keith Lindsay[8], Lixin Wu[1,9]

[1] School of Oceanography, Shanghai Jiao Tong University, Shanghai, China

[2] Open Studio for Ocean-Climate-Isotope Modeling, Pilot National Laboratory for Marine Science and Technology (Qingdao), Qingdao, China

[3] Atmospheric Science Program, Department of Geography, The Ohio State University, Columbus, OH, USA

[4] Department of Geology and Geophysics, Woods Hole Oceanographic Institution, Woods Hole, MA, USA

[5] School of Earth and Atmospheric Sciences, Georgia Institute of Technology, Atlanta, Georgia, USA

[6] Department for Atmospheric and Oceanic Sciences and Institute of Arctic and Alpine Research, University of Colorado Boulder, Boulder, CO, USA

[7]

[8] National Center for Atmospheric Research, Climate and Global Dynamics Division, Boulder, CO, USA

[9] Pilot National Laboratory for Marine Science and Technology (Qingdao), Qingdao, China

Correspondence authors: Sifan Gu (gusifan@sjtu.edu.cn), Zhengyu Liu (liu.7022@osu.edu)

This file contains additional information about the methods and additional figures to the main manuscript.

Text 1. Remineralized $\delta^{13}C$ estimation from AOU

The remineralized $\delta^{13}C$ in POP2 can be estimated from AOU (Sarmiento and Gruber, 1996) as described below. Total DIC, which is mostly $DI^{12}C$, can be seperated into preformed DIC (DIC_{pre}) and remineralized DIC (DIC_{remin}):

$$DIC = DIC_{pre} + DIC_{rem} \text{ (eq. 1)}$$

The fractionation in POP2 involves organic fractionation and carbonate formation (eq.2), therefore, DIC_{rem} can be further decomposed into DIC related to the organic process (DIC_{org}) and DIC related to carbonate pricipitation (DIC_{CaCO3}):

$$DIC_{rem} = DIC_{org} + DIC_{CaCO3} \text{ (eq. 2)}$$

DIC_{org} can be estimated using AOU by:

$$DIC_{org} = r_{C:O}*AOU \text{ (eq. 3)}$$

where $r_{C:O}$ is the ratio of carbon to oxygen during the organic process and is set to 117/138 in the model. DIC_{CaCO3} can be estimated as:

$DIC_{CaCO3} = (ALK - ALK_{pre} + r_{N:O}*AOU)/2$ (eq. 4),

where ALK is alklinity, ALK_{pre} is preformed alklinity, and $r_{N:O}$ is the ratio of nitrate to oxygen during the organic process which is 16/170. The ALK_{pre} can be estimated by:

$ALK_{pre} = (367.5 + 54.9*S + 0.074*(O_2 + r_{O:P}*PO_4))$ (eq. 5),

where S is salinity, O_2 is oxygen concentration, PO_4 is phosphate concentraion, and $r_{O:P}$ is the ratio of oxygen and phosphahte during the organic process which is 170. Combinating equation 1-5, the DIC_{pre} can be calculated by: $DIC_{pre} = DIC - DIC_{org} – DIC_{CaCO3}$ (eq. 6).

The fractionation during the organic process ($\delta^{13}C_{org}$) is approximately -21‰ and the fractionation during the carbonate precipitation ($\delta^{13}C_{CaCO3}$) is 2‰. Therefore, the $\delta^{13}C_{pre}$ can be calculated by:

$$\delta^{13}C_{pre} = (\delta^{13}C* DIC - \delta^{13}C_{org}*DIC_{org} - \delta^{13}C_{CaCO3}* DIC_{CaCO3})/DIC_{pre} \text{ (eq.7)}$$

and the $\delta^{13}C_{remin}$ can be estimated by $\delta^{13}C - \delta^{13}C_{pre}$.

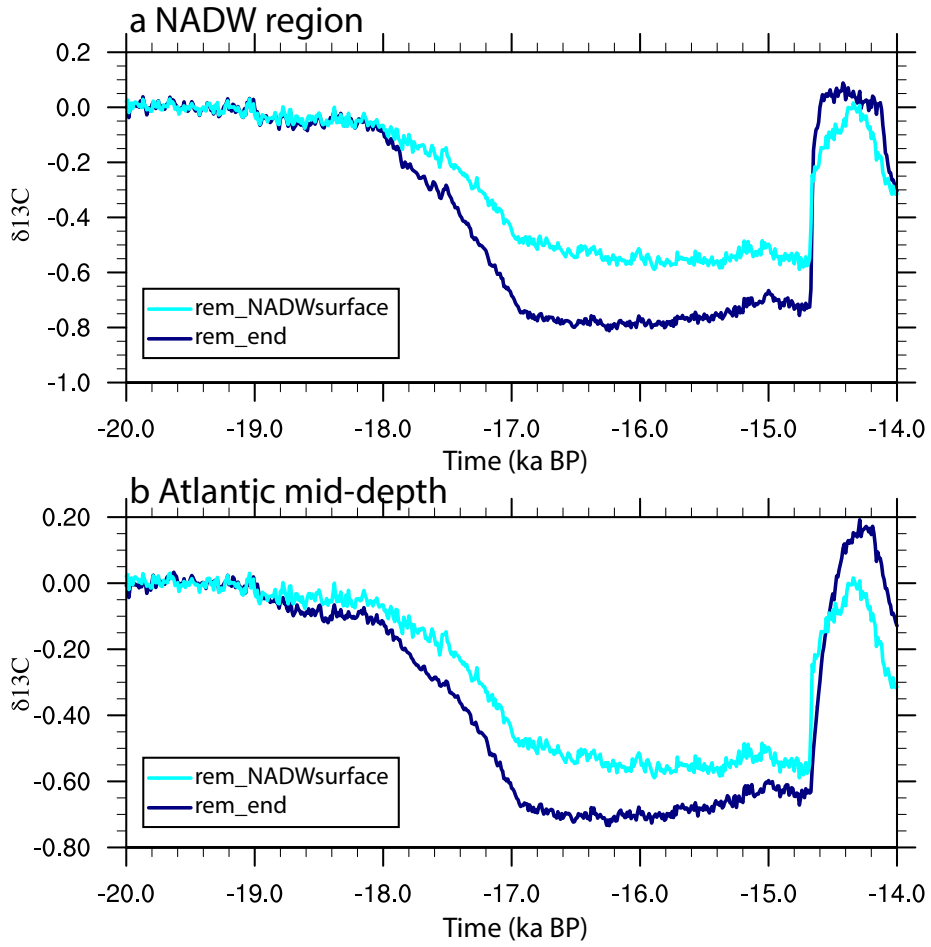

Figure S1. Validation of the $\delta^{13}C_{rem-end}$ estimation in NADW deep end-member region (a) and Atlantic mid-depth average (b): $\delta^{13}C_{rem-end}$ by the difference between $\delta^{13}C_{rem}$ and $\delta^{13}C_{rem-path}$ (navy); $\delta^{13}C_{rem}$ in the NADW surface end-member (light blue)

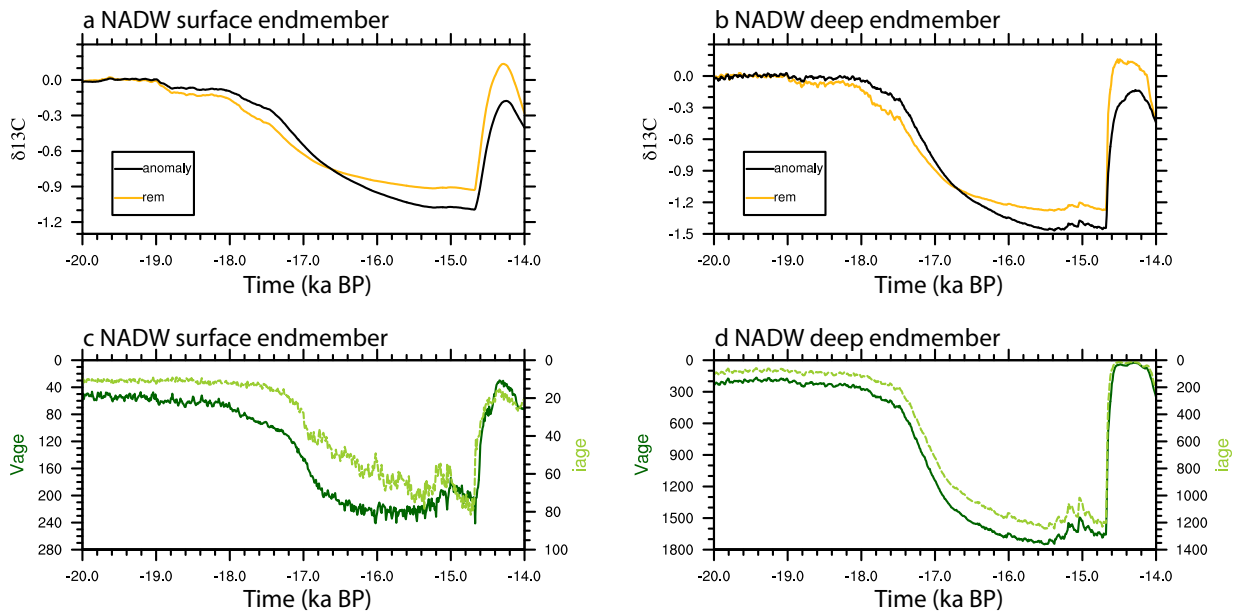

Figure S2. Evolutions in NADW surface and deep end-members. (a) $\delta^{13}C$ anomaly (black) and $\delta^{13}C_{rem}$ (yellow) of NADW surface end-member. (b) $\delta^{13}C$ anomaly (black) and $\delta^{13}C_{rem}$ (yellow) of NADW deep end-member. (c) Idealized ventilation age (dark solid green) and ideal age (light dashed green) in NADW surface endmember. (d) Idealized ventilation age (dark solid green) and ideal age (light dashed green) in NADW deep endmember.

Table S1. $\delta^{13}C$ observations used in model-data comparison.

site	Lat	lon	Depth (m)	$\delta^{13}C$ (HS1-LGM)	Reference
14GGC	-26.68	-46.5	441	0.0667	(Curry and Oppo, 2005)
90GGC	-27.35	-46.63	1105	0.332	(Curry and Oppo, 2005)
KNR159-5-36GGC	-27.27	-46.47	1268	0.14	(Curry and Oppo, 2005)
KNR159-5-17JPC	-27.7	-46.48	1627	-0.58	(Tessin and Lund, 2013)
KNR159-5-78GGC	-27.48	-46.33	1820	-0.48	(Tessin and Lund, 2013)
KNR159-5-33GGC	-27.57	-46.18	2082	-0.31	(Tessin and Lund, 2013)
KNR159-5-42JPC	-27.76	-46.63	2296	-0.32	(Curry and Oppo, 2005)
KNR159-5-73GGC	-27.89	-46.04	2397	-0.07	(Tessin and Lund, 2013)
KNR159-5-30GGC	-28.13	-46.04	2500	-0.19	(Tessin and Lund, 2013)

20JPC	-28.64	-45.54	2951	-0.2075	(Lund et al., 2015)
KNR159-5-125GGGC	-29.52	-45.75	3589	-0.2	(Hoffman and Lund, 2012)
KNR159-5-22GGGC	-29.79	-43.59	3924	0.15	(Hoffman and Lund, 2012)
GeoB3104-1	-3.66	-37.71	767	-0.008925	(Arz et al., 1999)
GS07-150-17	-4.21	-37.07	1000	-0.625	(Freeman et al., 2015)
GeoB16206-1	-1.58	-43.02	1367	-2.23	(Voigt et al., 2017)
GeoB1602-2	-1.91	-41.59	2247	-0.55769	(Mulitza et al., 2017)
GeoB3910-2	-4.25	-36.35	2362	-0.5842	(Burckel et al., 2015)
GeoB16224-1	6.65	-52.08	2510	-0.335833	(Voigt et al., 2017)
Rapid-10-1P	62.98	-17.59	1237	-0.86	(Thornalley et al., 2010)
EW9302-26GGC	62.32	-21.46	1450	-1.08	(Oppo et al., 2015)
EW9302-25GGC	62.06	-21.47	1523	-1.08	(Oppo et al., 2015)
NEAP4k	61.29	-24.17	1627	-0.88	(Rickaby and Elderfield, 2005)
EW9302-24GGC	62	-21.67	1629	-0.92	(Oppo et al., 2015)
ODP 984	61	-24	1648	-0.83	(Praetorius et al., 2008)
Rapid-15-4P	63.29	-17.13	2133	-0.27	(Thornalley et al., 2010)
RAPiD-17-5P	61.48	-19.54	2303	-0.38	(Thornalley et al., 2010)
KN166-14-JPC-13	53.06	-33.53	3082	-0.3	(Hodell et al., 2010)
IODP U1308	49.88	-24.24	3883	-0.25	(Hodell et al., 2008)

Reference:

Arz, H.W., Pätzold, J., Wefer, G., 1999. The deglacial history of the western tropical Atlantic as inferred from high resolution stable isotope records off northeastern Brazil. Earth Planet. Sci. Lett. 167, 105–117. https://doi.org/10.1016/S0012-821X(99)00025-4

Burckel, P., Waelbroeck, C., Gherardi, J.M., Pichat, S., Arz, H.W., Lippold, J., Dokken, T., Thil, F., 2015. Atlantic Ocean circulation changes preceded millennial tropical South America rainfall events during the last glacial. Geophys. Res. Lett. 42, 411–418. https://doi.org/10.1002/2014GL062512.Received

Curry, W.B., Oppo, D.W., 2005. Glacial water mass geometry and the distribution of δ13 C of ΣCO2 in the western Atlantic Ocean. Paleoceanography 20. https://doi.org/10.1029/2004PA001021

Freeman, E., Skinner, L.C., Tisserand, A., Dokken, T., Timmermann, A., Menviel, L., Friedrich,

T., 2015. An Atlantic-Pacific ventilation seesaw across the last deglaciation. Earth Planet. Sci. Lett. 424, 237–244. https://doi.org/10.1016/j.epsl.2015.05.032
Hodell, D.A., Channeil, J.E.T., Curtis, J.H., Romero, O.E., Röhl, U., 2008. Onset of "Hudson Strait" Heinrich events in the eastern North Atlantic at the end of the middle Pleistocene transition (~640 ka)? Paleoceanography 23, 1–16. https://doi.org/10.1029/2008PA001591
Hodell, D.A., Evans, H.F., Channell, J.E.T., Curtis, J.H., 2010. Phase relationships of North Atlantic ice-rafted debris and surface-deep climate proxies during the last glacial period. Quat. Sci. Rev. 29, 3875–3886. https://doi.org/10.1016/j.quascirev.2010.09.006
Hoffman, J.L., Lund, D.C., 2012. Refining the stable isotope budget for Antarctic Bottom Water: New foraminiferal data from the abyssal southwest Atlantic. Paleoceanography 27, 1–12. https://doi.org/10.1029/2011PA002216
Lund, D.C., Tessin, A.C., Hoffman, J.L., Schmittner, A., 2015. Southwest Atlantic water mass evolution during the last deglaciation. Paleoceanogr. Paleoclimatology 477–494. https://doi.org/10.1002/2014PA002657.Received
Mulitza, S., Chiessi, C.M., Schefuß, E., Lippold, J., Wichmann, D., Antz, B., Mackensen, A., Paul, A., Prange, M., Rehfeld, K., Werner, M., Bickert, T., Frank, N., Kuhnert, H., Lynch-Stieglitz, J., Portilho-Ramos, R.C., Sawakuchi, A.O., Schulz, M., Schwenk, T., Tiedemann, R., Vahlenkamp, M., Zhang, Y., 2017. Synchronous and proportional deglacial changes in Atlantic meridional overturning and northeast Brazilian precipitation. Paleoceanography 32, 622–633. https://doi.org/10.1002/2017PA003084
Oppo, D.W., Curry, W.B., McManus, J.F., 2015. What do benthic δ13C and δ18O data tell us about Atlantic circulation during Heinrich Stadial 1? Paleoceanography 30, 353–368. https://doi.org/10.1002/2014PA002667
Praetorius, S.K., McManus, J.F., Oppo, D.W., Curry, W.B., 2008. Episodic reductions in bottom-water currents since the last ice age. Nat. Geosci. 1, 449–452. https://doi.org/10.1038/ngeo227
Rickaby, R.E.M., Elderfield, H., 2005. Evidence from the high-latitude North Atlantic for variations in Antarctic Intermediate water flow during the last deglaciation. Geochemistry, Geophys. Geosystems 6. https://doi.org/10.1029/2004GC000858
Sarmiento, J.L., Gruber, N., 1996. Ocean Biogeochemical Dynamics.
Tessin, A.C., Lund, D.C., 2013. Isotopically depleted carbon in the mid-depth South Atlantic during the last deglaciation. Paleoceanography 28, 296–306. https://doi.org/10.1002/palo.20026
Thornalley, D.J.R., Elderfield, H., McCave, I.N., 2010. Intermediate and deep water paleoceanography of the northern North Atlantic over the past 21,000 years. Paleoceanography 25, PA1211. https://doi.org/10.1029/2009PA001833
Voigt, I., Cruz, A.P.S., Mulitza, S., Chiessi, C.M., Mackensen, A., Lippold, J., 2017. Variability in mid-depth ventilation of the western Atlantic Ocean during the last deglaciation. Palaeogeography 32, 1–27. https://doi.org/10.1002/2017PA003095